Reversible Switching of Interlayer Exchange Coupling through Atomically Thin VO2 via Electronic State Modulation

Xiaofei Fan, Guodong Wei, Xiaoyang Lin, Xinhe Wang, Zhizhong Si, Xueying Zhang, Qiming Shao, Stéphane Mangin, Eric E. Fullerton, Lei Jiang, et al.

Reversible Switching of Interlayer Exchange Coupling through Atomically-thin VO_2 via Electronic State Modulation

Xiaofei Fan,[1,7] Guodong Wei,[1,7] Xiaoyang Lin,[1,2,*] Xinhe Wang,[1] Zhizhong Si,[1] Xueying Zhang,[1,2] Qiming Shao,[3] Stéphane Mangin,[4] Eric Fullerton,[5] Lei Jiang,[6] Weisheng Zhao[1,2,8,*]

[1] Fert Beijing Research Institute, School of Microelectronics & Beijing Advanced Innovation Center for Big Data and Brain Computing (BDBC), Beihang University, Beijing 100191, China

[2] Beihang-Goertek Joint Microelectronics Institute, Qingdao Research Institute, Beihang University, Qingdao 266000, China

[3] Department of Electronic and Computer Engineering, The Hong Kong University of Science and Technology, Clear Water Bay, Kowloon, Hong Kong SAR, China

[4] Institut Jean Lamour, UMR 7198, CNRS-Université de Lorraine, F-54000 Nancy, France

[5] Center for Memory and Recording Research, University of California San Diego, 9500 Gilman Drive, La Jolla, CA 92093-0401, USA

[6] School of Chemistry, Beihang University, Beijing 100191, China

[7] These two authors contributed equally.

[8] Lead Contact

*Correspondence:

XYLin@buaa.edu.cn (X.Y.L), weisheng.zhao@buaa.edu.cn (W.S.Z)

Summary

Modulation of electronic properties in spintronic interfaces (spinterfaces) can give rise to the optimization and even emergence of abundant spintronic effects. However, a proof-of-concept demonstration of such a strategy has rarely been achieved. In this paper, we study the interlayer exchange coupling effect in a synthetic magnetic multilayer system $[Pt/Co]_2/VO_2/[Co/Pt]_2$, where atomically-thin phase change material VO_2 is adopted as a spinterface with reversible metal-to-insulator transition. Repeatable switching from antiferromagnetic coupling through insulating spinterface to ferromagnetic coupling through metallic spinterface is observed in this multilayer system. Further analyses indicate that such an evolution originates from two distinct coupling mechanisms of spin dependent tunneling and Rudermann–Kittel–Kasuya–Yosida interaction determined by the electronic states of VO_2. As an experimental demonstration of VO_2-tailored interlayer exchange coupling effect, this work highlights the great potential of spinterface as a magic building block in beyond-CMOS electronic devices.

Keywords: spinterface; phase change; interlayer exchange coupling; vanadium dioxide; spintronics

Introduction

Using electron spin states as quantum information carriers opens a broad avenue for storage, sensing and computing, known as the spintronics[1]. The spintronic property of a heterostructure is not only determined by the ferromagnetic electrodes via spin-dependent scattering, but also influenced remarkably by the spintronic interface (spinterface)[2–4], which tailors the physical process of spin filtering[5], hot-electron transport[6], spin torques[7–10] and interfacial Dzyaloshinskii-Moriya interaction[11,12] etc. Previous studies reveal that the electronic property engineering of spinterfaces can become an effective strategy to extraordinarily optimize these physical effects and turn them into practical applications[10,12]. In this regard, spinterfaces with dramatically changeable electronic properties can be a magic building block for beyond-CMOS electronics.

As a representative effect of spinterface-tailored physical effects, interlayer exchange coupling (IEC) describes indirect interactions between magnetic layers through an atomically-thin spacer[3,10,13]. The coupling type, *e.g.*, ferromagnetic (FM) or antiferromagnetic (AFM), reflects the band structure of the spacer around the Fermi surface[14–16]. For IEC through metallic spacers, the periodic oscillation and fast decay of coupling strength with the spacer thickness[17] have been explained by Rudermann–Kittel–Kasuya–Yosida (RKKY) theory[18], which originates from interactions between localized d- or f-orbit electrons via the conduction electrons. Meanwhile, theories such as variable-range hopping and resonant tunneling through defect-generated localized electronic states in the gap of barrier have been developed to explain the exchange coupling through semiconducting spacers[19,20]. For insulating spacers, IEC with appreciable

strength and absence of oscillation has been interpreted by the spin dependent tunneling[21,22]. Pioneering theoretical studies have also been performed to develop a unified theory for different kinds of spacers by introducing the concept of a complex Fermi surface[23]. Thus, IEC through spacers with controllable electronic properties, such as phase change materials[24], can be a good choice to demonstrate the extraordinary control of physical effects tailored by the spinterface.

In this work, we study the IEC evolution through an atomically-thin VO_2 spacer, which features a metal-insulator transition during the phase change[25,26]. Magnetic heterostructure samples of $[Pt/Co]_2/VO_2/[Co/Pt]_2$ with perpendicular magnetic anisotropy (PMA) are prepared by magnetron sputtering under high vacuum to explore the electronic state induced regulation on the IEC. Reversible switching between AFM coupling through insulating VO_2 and FM coupling through metallic VO_2 is observed. The IEC regulation behavior is further explained by the effect of band structure change in VO_2, where the coupling mechanism changes from spin dependent tunneling to RKKY interaction. Such an *in-situ* IEC control may give rise to extended tunability of many magnetic devices, such as magnetic random-access memory, highly sensitive magnetic sensors and spin torque nano-oscillators, which is potential for function innovations of them. In addition to extending the platforms for *in-situ* IEC control, this work, based on electronic state modulations of the VO_2 spinterface, may provide a widely-applicable, all-solid and multiply triggered solution to optimize spintronic effects and implement device functions[27].

Results

Atomically-thin VO_2 films and phase change magnetic heterostructures

The indirect coupling nature of IEC features a fast decay of the coupling strength with the spacer thickness, which usually confines the critical thickness of the spacer below several nanometers[17]. For experimental explorations of electronic state induced IEC regulation, the preparation of atomically-thin VO_2 films is thus a fundamental problem. Although many methods have been developed to deposit VO_2, such as molecular beam epitaxy[28], pulsed laser deposition[29] and chemical vapor deposition[30], strict growth conditions, *e.g.*, specific substrates, high temperature and high oxygen pressure, limit their applications in spintronics[25]. A deposition method with abilities of nanometer-accuracy, heterostructure integration and interface engineering is thus desired.

In this work, magnetron sputtering is chosen as the deposition method of VO_2 and relevant magnetic heterostructures. Through a careful optimization of the deposition conditions, atomically-thin VO_2 films with nanometer thicknesses can be successfully prepared under high vacuum at room temperature. A broad peak has been found in the X-ray diffraction (XRD) result, indicating their amorphous feature (see Supplementary **Figure S1**). X-ray photoelectron spectroscopy (XPS) measurement is applied to check the valence state of vanadium. As shown in **Figure 1A**, the proportion of VO_2 reaches 97%, which demonstrates the relatively pure composition. The I-V curves with increasing temperature of a vertical tunnel junction device fabricated based on Au/VO_2 (2 nm)/Au heterostructure are shown in **Figure 1B**, from which an evolution from a tunneling contact to a transparent contact can be detected. The results indicate the dramatic change of the electronic property (*i.e.*, an insulator to metal transition) in the VO_2

spacer when the thermally triggered phase change occurs. Similar transport measurements of tunnel junctions with varied VO_2 thickness can be found in **Figure S2. Figure 1C** presents the ratio of the resistance change (calculated as the resistance divided by its minimum value) versus temperature with a measured current of 10 nA for a 2-nm-thick sample and a 40-nm-thick single-crystal film sample. It is noteworthy that the metal-insulator transition in the atomically-thin VO_2 layer occurs at a temperature much lower than that of the bulk sample. This difference is probably caused by the effect of interfacial strain, interfacial bonds or defects[25]. Although potential factors such as the amorphous nature and inevitable defects still affect the resistance change amplitude (~20 times), the hysteresis phenomenon proves the existence of the metal-insulator transition in the atomically-thin film.

The appreciable metal-insulator transition, good compatibility of the substrates and high vacuum room-temperature deposition conditions of the atomically-thin VO_2 film further enable the fabrication of VO_2-based magnetic heterostructures. To investigate the effect of spinterface-tailored IEC, we prepare a series of $[Pt/Co]_2/VO_2/[Co/Pt]_2$ heterostructures (see **Figure 1D** for a schematic diagram). VO_2 layers with different thickness are adopted as the spacers, and Co/Pt systems are chosen as the FM layers with PMA. Distinct interfaces between multilayers are verified by high-resolution transmission electron microscopy (HRTEM, see **Figure 1E**), by which the thicknesses of the atomically-thin VO_2 spacers are calibrated to be 0.76, 1.48, 1.83 and 2.26 nm (see **Figure S3**). Some regions with microcrystalline morphology can also be observed within the VO_2 layer, which may be caused by the fluctuations of the sputtering energy and non-

annealing process. These inevitable defects can explain the sluggish metal-insulator transition curve and non-uniform phase change process mentioned in the following discussion. In the VO_2-based magnetic heterostructures, the magnetic electrons in the top and bottom layers are coupled indirectly through atomically-thin VO_2, whose electron density of 3d orbitals varies tremendously during the metal-insulator transition. Considering the process of electron reflections between the two electrodes in the spacer, this variation not only influences the transport efficiency which alters the magnitude of the electron wave, but also changes the phase shift during the reflecting. As a result, the quantum well states of the system will be altered, which determines the energy favorable coupling state[23]. An unrevealed evolution of the IEC can thus be expected owing to the dramatic change in the VO_2 spinterface (**Figure 1F**).

Electronic state induced IEC regulation

The IEC regulation in the phase change magnetic heterostructures is firstly investigated by magnetic property measurements. A vibrating sample magnetometer (VSM) is used to characterize the $[Pt/Co]_2/VO_2/[Co/Pt]_2$ samples. As shown in **Figure 2A**, strong anisotropy is detected in the sample with a 0.76-nm-thick VO_2 spacer. Similar PMA properties can be found in all the other films (see **Figure S4**). The magnetization shows two reorientation processes depending on the magnetic field, which indicates strong FM coupling within both the top and bottom Co/Pt bilayers. Thus, these bilayers will be treated as two single FM units when investigating the spinterface-tailored IEC effect.

As illustrated in **Figures 2B-2E**, hysteresis loops are also measured by the polar magneto-optic Kerr microscope (p-MOKE) before and after the metal-insulator transition for samples with different thickness of VO_2. Interestingly, the two magnetization flips merge into one after the VO_2 spacer change to be conducting for the 0.76-, 1.48-, 1.83- and 2.26-nm-thick VO_2 spacer samples. The experimental results of the control samples (with the structure of $[Pt/Co]_2/VO_2$ and $VO_2/[Co/Pt]_2$, **Figure S5**) show that the magnetization reorientation fields of the two Co/Pt bilayers are always different during the metal-insulator transition. Additionally, the phase change magnetic heterostructure shows no indication of anisotropy change, as the in-plane hysteresis loops coincide with each other during the metal-insulator transition (**Figure 2F** and **Figure S6**). These features thus exclude the possibility that the regulation is caused by the differentiated PMA modulation effect on the top and bottom magnetic layers, and especially confirm the appearance of strong FM coupling between top and bottom Co/Pt bilayers when the atomically-thin VO_2 spacer becomes metallic.

To further understand this IEC regulation via dynamic modulation of the electronic states in VO_2 spacer, one key issue is to distinguish the coupling state of the $[Pt/Co]_2/VO_2/[Co/Pt]_2$ samples when VO_2 is insulating. Taking the sample with 0.76-nm-thick VO_2 as an example, a high-accuracy VSM with a built-in Hall probe (detecting accuracy of 0.01 Oe) is applied to collect the minor loop of the top magnetic layer. As shown in **Figure 3A**, a positive exchange bias $H_{ex\text{-}top}$ (~0.35 Oe) can be detected in multiple measurements at room temperature. Further result shows that the value increases to 0.64 Oe when temperature is decreased to 200K, indicating the

existence of an AFM coupling through insulating VO_2. To further confirm this result, the magnetic domain switching behavior around the field region of the minor loop is also investigated, as shown in **Figure 3B**. The results verify that the domain switching of the top magnetic layer happens near -0.2 Oe and 1.88 Oe, also giving a positive value of $H_{ex\text{-}top}$. Meanwhile, similar minor loop measurements are carried out for other samples (see **Figure S7**), which suggest that the samples with 1.48-, 1.83-, and 2.26-nm-thick VO_2 also exhibit AFM coupling for insulating VO_2 ($H_{ex\text{-}top}$=0.57, 0.56 and 0.59 Oe, respectively). However, when the thickness of VO_2 spacer is greater than 3 nm, the sample exhibits a decoupling feature ($H_{ex\text{-}top}$≈0.00 Oe), which meets the fast decay feature of IEC. The dipolar effect, caused by the stray field of FM layers around the rough interfaces, can also result in 'fake' coupling. However, the HRTEM evidence of perfectly smooth interfaces (see Supplementary **Figure S3E**) indicates neglectable influence of this effect.

To obtain more details about the regulation effect, we then focus on the evolution of the IEC during the dynamic metal-insulator transition of VO_2 triggered by temperature control. **Figure 3C** shows the hysteresis loops of the samples at different temperatures. In all the four samples, there are double flips in the loops with insulating VO_2. As the electronic property changing from insulator to metal occurs, the loops feature a smooth flip of the top FM layer before a sudden transition into one single flip (that is, strong FM coupling). Interestingly, the critical temperature of the change in the IEC type shows a clear dependence on the VO_2 thickness. For the two thinner samples (0.76 nm and 1.48 nm), FM coupling appears around 320 K, while for the two

thicker samples (1.83 nm and 2.26 nm), the FM coupling change occurs at a slightly lower temperature (approximately 310 K). Considering the similar deposition parameters of all samples, one possible reason for this difference is the appreciable interfacial strain effect on the metal-insulator transition temperature of the atomically-thin VO_2[25]. Considering that the VO_2 exhibits obvious hysteresis of metal-insulator transition (**Figure 1C**), the electronic state induced IEC regulation should exhibit the same feature. Therefore, we measure the magnetic loops of the 0.76-nm-thick VO_2 sample at two temperatures within the hysteresis range (305 and 315 K) during insulator to metal and metal to insulator transition processes (*i.e.*, heating-up and cooling-down). As shown in **Figure 3D**, the sharpness of the flip in both results shows a clear difference, which proves our speculation and further verifies the origin of the IEC regulation as the metal-insulator transition of VO_2. Further measurements (**see Figure S8**) indicate the excellent repeatability of the AFM-to-FM coupling transition in these samples.

Based on the results obtained from all VO_2-based magnetic heterostructures, the exchange bias between two FM layers can be derived from the center shift of minor loops (for example the $H_{ex\text{-}top}$ in **Figure 3A**) or the shift of the flip edges relative to those of control samples[31]. Considering the canted shape of the minor loops at high temperatures, we use the difference between the flip edge of the bottom FM layer (**Figure 3C**) and the coercive field of VO_2/$[Co/Pt]_2$ control sample (**Figure S9**) to calculate the value of exchange bias field $H_{ex\text{-}bottom}$. There are also some reports about the presence of AFM ordering with insulating VO_2[32]. The calculation rule can thus eliminate this influence in the process of mutual subtraction. As plotted in **Figure 4A**, the negative $H_{ex\text{-}}$

$_{bottom}$ values represent AFM coupling, and the positive represent FM coupling. Samples with various thickness of VO_2 (0.76, 1.48, 1.83 and 2.26 nm) all demonstrate a transition from appreciable AFM coupling through insulating VO_2 spinterface to stronger FM coupling through metallic VO_2 spinterface.

Physical origin of the electronic state induced IEC regulation

Considering the complexity of the spinterface, the mechanism behind the regulation can be a combined result of various effects, including the variation in electronic state, interfacial strain, Co-O bonds and interface defects etc. during the phase change. However, as the VO_2 layer is amorphous, it is hard to form a uniform strain to have a long-range effect on the exchange coupling. For Co-O bonds or interface defects, the affected atoms are usually confined around the interface limited in a few angstroms,[33,34] which is far thinner than the Co/Pt bilayer thickness. Additionally, the magnetic anisotropy which is sensitive to these influences remains unchanged in the regulation process (**Figure 2F**), which indicates that they are not the major determinants. Since the IEC change shows a high correlation with phase change of VO_2 (**Figure 3C** & **3D**), it is more convincing to attribute such a reversible coupling change to electronic state modulations of VO_2.

To understand the possible mechanism, the phase change of VO_2 should be taken into consideration. As pointed out by Goodenough, the Peierl-like phase change of VO_2 can produce a large spectral weight transfer from π* (d_{xy}) orbitals into the valence $d_{//}$ ($d_{xz,\ yz}$) orbitals and

eliminate the band gap[32,35]. The distinct electronic states of VO_2 can thus cause different IEC origins and behaviors. To clarify the physical mechanism of IEC through insulating and metallic VO_2 spinterface, the dependence of the coupling strength on VO_2 thickness at 200 and 360 K is shown in **Figure 4B**. The experimental values of coupling strength J_{exp} are determined from the exchange bias field $H_{ex\text{-}bottom}$ using the relation [31],

$$J_{\exp} = H_{ex-\text{bottom}}\left(M_{S1}t_1 M_{S2}t_2\right)/\left(M_{S1}t_1 + M_{S2}t_2\right), \qquad \text{(Equation 1)}$$

where t_1 (0.9 nm) and t_2 (2 nm) represent the thicknesses of Co layers in the top and bottom magnetic layers, respectively, and M_{S1} and M_{S2} are their saturation magnetizations.

For IEC via insulating VO_2 spinterface, the rapid decay of the coupling strength with thicker spacer is consistent with the trend observed in oxide–based synthetic antiferromagnets[21]. Considering the tunneling feature in the transport measurement of Au/VO_2/Au junctions (**Figure 1B & Figure S2**), spin dependent tunneling, as suggested for the Co/MgO/Co system[36], which also features an exponential coupling strength decay, should dominate IEC in this case. The coupling strength then can be calculated as[22]:

$$J_{cal} = \frac{(U - E_F)}{8\pi^2 d^2} \frac{8k^3(k^2 - k_\uparrow k_\downarrow)(k_\uparrow - k_\downarrow)^2(k_\uparrow + k_\downarrow)}{(k^2 + k_\downarrow^2)^2(k^2 + k_\uparrow^2)^2} e^{-2kd}, \qquad \text{(Equation 2)}$$

Where J_{cal} is the calculated coupling strength, $(U\text{-}E_F)$ gives the barrier height of the heterostructure, $k_\uparrow$, $k_\downarrow$ is the Fermi wave vectors for the spin up and down bands of the FM layers, d is the thickness of the insulating spacer, and k is the wave vectors of electrons in the insulating layer,

$$k^2 = \frac{2m_{\text{eff}}(U - E_F)}{\hbar^2}, \qquad \text{(Equation 3)}$$

A barrier height value of 1 eV, referring to the work function of VO_2 and Co[37], and an effective electron mass m_{eff}=1 m_e[38], are adopted to perform the fitting of J_{cal} in **Figure 4B**, which perfectly coincides with the experimental results of IEC through insulating VO_2 (at 200 K). Notably, the coupling strength shows a comparable value at AFM state to that of the FM state. According to previous research[39], localized states within the band gap induced by defects can enhance the coupling by spin dependent tunneling, and feature a strength decrease with temperature rising. Such an interpretation is consistent with the amorphous feature of the atomically-thin VO_2 films (**Figure 1E**) and the temperature dependence of the exchange field at AFM state (**Figure 4A**).

For the FM coupling via metallic VO_2 spinterface, the most widely accepted coupling mechanism is RKKY interaction. The coupling strength then can be calculated as[40]:

$$J_{cal} \approx \frac{9\pi\delta^2\upsilon^2 F(\xi)}{64E_F}, \qquad \text{(Equation 4)}$$

where δ is the coupling constant, υ is the number of conduction electrons per atom, E_F is the Fermi energy and $F(\xi)$ is the RKKY function[40]

$$F(\xi) = (\sin\xi - \xi\cos\xi)/\xi^4, \qquad \text{(Equation 5)}$$

where $\xi = 2k_F d$. The Fermi wavevector of free electrons k_F is fitted to be $1.4*10^7$ m^{-1} in the case of metallic VO_2 at 350 K. It appears clearly in **Figure 4B** that the experimental variation of the coupling strength with the metallic VO_2 spacer is well fitted with the framework of the RKKY model. Following the RKKY mechanism, the IEC through metallic VO_2 has a characteristic

feature of an extremely large oscillation period (up to hundreds of nanometers, see Inset of **Figure 4B**). As an example, an FM coupling of 37 μerg/cm^3 can still be detected through a metallic VO_2 when its thickness reaches 3.22 nm. However, the coupling of this sample with insulating VO_2 is almost undetectable.

Besides the AFM to FM transition, the IEC evolution in our results accompanied by the smoothing of the first magnetization flip is different from a mere flip approaching behavior in a uniform IEC change route (**Figure 4C**). It can be explained by the inhomogeneous feature of the amorphous atomically-thin VO_2 film[41], which could induce domains with different conductivity and thus non-uniform coupling during the metal-insulator transition. This speculation is confirmed by the Kerr microscope of the domain at critical switching state during the insulator to metal transition, which first evolves into a maze morphology, then finely breaks into smaller size beyond the resolution of the microscope (**Figure 4D**). With the in-plane loop measurement excluding the possibility of an anisotropy change (**Figure 2F** and **Figure S6**), it is reasonable to believe that this change is caused by the non-uniform phase change of VO_2 providing more nucleation points for spin switching.

Discussion

Overall, the IEC regulation in this work has been verified to get tailored by the electronic state of the VO_2 spinterface. Compared to the modulation based on strain[42] or ion migration[14,15], such a pure electronic effect features the potential advantages of high stability, low power consumption,

high speed (if with photonic excitation strategy[43]) and all-solid structure. Such a VO_2 based spinterface, with appreciable metal-insulator transition that can be induced by methods such as thermal heating[25], electrical gating[25], and especially pulse laser excitation[43], would be a magic building block for spinterface-tailored physical effects and device applications. As the spinterface plays an important role in abundant physical processes, in addition to IEC, it is reasonable to believe that such a modulation method can be used to control other spin electronic structures or magnetic materials, such as skyrmion, 2D ferromagnets and ferromagnetic insulators. After proving the close relationship between IEC and interlayer electronic state by this work, further realization of phase change by electrical methods will give birth to even richer applications in spintronics.

Conclusion

In conclusion, atomically-thin VO_2 has been adopted as a spinterface with dramatically changeable electronic properties to regulate the interlayer exchange coupling effect. Both the coupling strength and the type (*that is*, antiferromagnetic and ferromagnetic coupling) of the magnetic heterostructures $[Pt/Co]_2/VO_2/[Co/Pt]_2$ can be tailored reversibly and repeatably through the metal-insulator transition of VO_2. Further analyses indicate that such an evolution originates from two distinct physical mechanisms of spin dependent tunneling and RKKY interaction determined by the electronic states of VO_2. As a proof-of-concept demonstration of interface-tailored spintronics, this work might provide a general strategy for beyond-CMOS electronics.

Experimental Procedures

Resource Availability:

Lead Contact: Further information and requests for resources and reagents should be directed to and will be fulfilled by the Lead Contact, Weisheng Zhao (weisheng.zhao@buaa.edu.cn).

Materials Availability: This study did not generate new unique reagents.

Data and Code Availability: Data supporting the findings of this manuscript are available from the corresponding authors upon reasonable request. A reporting summary for this article is available as a Supplemental Information file.

Film deposition and device fabrication： The Au/VO_2/Au and $[Pt/Co]_2/VO_2/[Co/Pt]_2$ heterostructures were both grown on SiO_2/Si substrates by magnetron sputtering at room temperature under high vacuum. A stoichiometric target was used to deposit the VO_2 film during the experiments. The tunnel junctions were patterned by optical lithography (Micro Writer ML Baby, Durham Magneto Optics) followed by argon ion-beam etching of the bottom electrodes and pillars. Then, the samples were fully covered with SiO_2 for insulation. After etching, a series of vias were produced over the pillars to ensure the connection between the junction and the top electrodes. Both the bottom electrodes and tunnel junctions were then connected to 90-nm Ti/Au electrodes using e-beam evaporation to allow electrical contact for the measurements.

Characterization and measurement： The magnetic properties were measured by the MOKE (NanoMOKE3, Durham Magneto optics ltd) with a homemade heat source and a VSM (7400, Lakeshore) at different temperatures. The Au/VO_2/Au tunnel junctions were measured by normal 4-terminal methods with Keithley 6221 and Keithley 2182 source and measurements units, respectively. HRTEM was performed by a Talos F200X instrument. The XPS results were obtained by a Thermo Fisher ESCALAB 250Xi instrument, and the XRD measurements were performed by a Delta-X instrument.

Acknowledgments

We thank Prof. Albert Fert & Prof. Dapeng Zhu for helpful discussions. This work was supported by the National Natural Science Foundation of China (No. 51602013, 11804016, and 61627813), Young Elite Scientists Sponsorship Program by China Association for Science and Technology (CAST) (No. 2018QNRC001), the International Collaboration 111 Project (No. B16001), the Fundamental Research Funds for the Central Universities of China, and the Beijing Advanced Innovation Centre for Big Data and Brain Computing (BDBC), the French PIA project Lorraine Université d'Excellence, reference ANR-15-IDEX-0004, ICEEL and by Feder EU.

Author contributions

Conceptualization, X.Y.L. and W.S.Z.; Methodology, X.Y.L. and S. M.; Investigation, G.D.W. X.F.F., X.H.W., Z.Z.S., X.Y.Z. and X.Y.L.; Writing – Original Draft, G.D.W. X.F.F. and X.Y.L.; Writing – Review & Editing, G.D.W., X.Y.L., Q. S., S. M., E. F. and W.S.Z.; Resources, X.Y.L.,

W.S.Z., and L. J.; Funding Acquisition, X.Y.L., G.D.W., and W.S.Z.; Supervision, X.Y.L., and W.S.Z.

Declaration of Interests: The authors declare no competing interests.

References and Notes

1. Bader, S.D., and Parkin, S.S.P. (2010). Spintronics. Annu. Rev. Condens. Matter Phys. *1*, 71–88.
2. Hellman, F., Hoffmann, A., Tserkovnyak, Y., Beach, G.S.D., Fullerton, E.E., Leighton, C., MacDonald, A.H., Ralph, D.C., Arena, D.A., Dürr, H.A., et al. (2017). Interface-induced phenomena in magnetism. Rev. Mod. Phys. *89*, 025006.
3. Lin, X., Yang, W., Wang, K.L., and Zhao, W. (2019). Two-dimensional spintronics for low-power electronics. Nat. Electron. *2*, 274–283.
4. De Teresa, J.M., Barthélémy, A., Fert, A., Contour, J.P., Montaigne, F., and Seneor, P. (1999). Role of Metal-Oxide Interface in Determining the Spin Polarization of Magnetic Tunnel Junctions. Science *286*, 507–509.
5. Parkin, S.S.P., Kaiser, C., Panchula, A., Rice, P.M., Hughes, B., Samant, M., and Yang, S.-H. (2004). Giant tunnelling magnetoresistance at room temperature with MgO (100) tunnel barriers. Nat. Mater. *3*, 862–867.
6. Kurnosikov, O., de Jong, J.E.A., Swagten, H.J.M., and de Jonge, W.J.M. (2002). Direct observation of local hot electron transport through Al_2O_3 tunnel junctions. Appl. Phys. Lett.

80, 1076–1078.

7. Sato, N., Xue, F., White, R.M., Bi, C., and Wang, S.X. (2018). Two-terminal spin–orbit torque magnetoresistive random access memory. Nat. Electron. *1*, 508–511.

8. Xie, Q., Lin, W., Yang, B., Shu, X., Chen, S., Liu, L., Yu, X., Breese, M.B.H., Zhou, T., Yang, M., et al. (2019). Giant Enhancements of Perpendicular Magnetic Anisotropy and Spin–Orbit Torque by a MoS_2 Layer. Adv. Mater. *31*, 1900776.

9. Soumyanarayanan, A., Reyren, N., Fert, A., and Panagopoulos, C. (2016). Emergent phenomena induced by spin–orbit coupling at surfaces and interfaces. Nature *539*, 509–517.

10. Wang, M., Cai, W., Zhu, D., Wang, Z., Kan, J., Zhao, Z., Cao, K., Wang, Z., Zhang, Y., Zhang, T., et al. (2018). Field-free switching of a perpendicular magnetic tunnel junction through the interplay of spin–orbit and spin-transfer torques. Nat. Electron. *1*, 582–588.

11. Yang, H., Chen, G., Cotta, A.A.C., N'Diaye, A.T., Nikolaev, S.A., Soares, E.A., Macedo, W.A.A., Liu, K., Schmid, A.K., Fert, A., et al. (2018). Significant Dzyaloshinskii–Moriya interaction at graphene–ferromagnet interfaces due to the Rashba effect. Nat. Mater. *17*, 605–609.

12. Fernández-Pacheco, A., Vedmedenko, E., Ummelen, F., Mansell, R., Petit, D., and Cowburn, R.P. (2019). Symmetry-breaking interlayer Dzyaloshinskii–Moriya interactions in synthetic antiferromagnets. Nat. Mater. *18*, 679–684.

13. Han, D.-S., Lee, K., Hanke, J.-P., Mokrousov, Y., Kim, K.-W., Yoo, W., van Hees, Y.L.W., Kim, T.-W., Lavrijsen, R., You, C.-Y., et al. (2019). Long-range chiral exchange interaction

in synthetic antiferromagnets. Nat. Mater. *18*, 703–708.

14. Yang, Q., Wang, L., Zhou, Z., Wang, L., Zhang, Y., Zhao, S., Dong, G., Cheng, Y., Min, T., Hu, Z., et al. (2018). Ionic liquid gating control of RKKY interaction in FeCoB/Ru/FeCoB and $(Pt/Co)_2/Ru/(Co/Pt)_2$ multilayers. Nat. Commun. *9*, 991.

15. Newhouse-Illige, T., Liu, Y., Xu, M., Reifsnyder Hickey, D., Kundu, A., Almasi, H., Bi, C., Wang, X., Freeland, J.W., Keavney, D.J., et al. (2017). Voltage-controlled interlayer coupling in perpendicularly magnetized magnetic tunnel junctions. Nat. Commun. *8*, 15232.

16. Liu, P., Lin, X., Xu, Y., Zhang, B., Si, Z., Cao, K., Wei, J., and Zhao, W. (2017). Optically tunable magnetoresistance effect: From mechanism to novel device application. Materials. *11*, 47.

17. Parkin, S.S.P., More, N., and Roche, K.P. (1990). Oscillations in exchange coupling and magnetoresistance in metallic superlattice structures: Co/Ru, Co/Cr, and Fe/Cr. Phys. Rev. Lett. *64*, 2304–2307.

18. Ruderman, M.A., and Kittel, C. (1954). Indirect Exchange Coupling of Nuclear Magnetic Moments by Conduction Electrons. Phys. Rev. *96*, 99–102.

19. Inomata, K., Yusu, K., and Saito, Y. (1995). Magnetoresistance Associated with Antiferromagnetic Interlayer Coupling Spaced by a Semiconductor in Fe/Si Multilayers. Phys. Rev. Lett. *74*, 1863–1866.

20. Gareev, R.R., Bürgler, D.E., Buchmeier, M., Olligs, D., Schreiber, R., and Grünberg, P. (2001). Metallic-Type Oscillatory Interlayer Exchange Coupling across an Epitaxial FeSi Spacer. Phys. Rev. Lett. *87*, 157202.

21. Chen, B., Xu, H., Ma, C., Mattauch, S., Lan, D., Jin, F., Guo, Z., Wan, S., Chen, P., Gao, G., et al. (2017). All-oxide–based synthetic antiferromagnets exhibiting layer-resolved magnetization reversal. Science *357*, 191–194.

22. Faure-Vincent, J., Tiusan, C., Bellouard, C., Popova, E., Hehn, M., Montaigne, F., and Schuhl, A. (2002). Interlayer Magnetic Coupling Interactions of Two Ferromagnetic Layers by Spin Polarized Tunneling. Phys. Rev. Lett. *89*, 107206.

23. Bruno, P. (1995). Theory of interlayer magnetic coupling. Phys. Rev. B *52*, 411–439.

24. Nakano, M., Shibuya, K., Okuyama, D., Hatano, T., Ono, S., Kawasaki, M., Iwasa, Y., and Tokura, Y. (2012). Collective bulk carrier delocalization driven by electrostatic surface charge accumulation. Nature *487*, 459–462.

25. Liu, K., Lee, S., Yang, S., Delaire, O., and Wu, J. (2018). Recent progresses on physics and applications of vanadium dioxide. Mater. Today *21*, 875–896.

26. Wei, G., Lin, X., Si, Z., Lei, N., Chen, Y., Eimer, S., and Zhao, W. (2019). Phase-transition-induced large magnetic anisotropy change in VO_2/$(Co/Pt)_2$ heterostructure. Appl. Phys. Lett. *114*, 012407.

27. Wei, G., Lin, X., Si, Z., Wang, D., Wang, X., Fan, X., Deng, K., Liu, K., Jiang, K., Lei, N., et al. (2020). Optically Induced Phase Change for Magnetoresistance Modulation. Adv. Quantum Technol. *1900104*, 1900104.

28. Fan, L.L., Chen, S., Wu, Y.F., Chen, F.H., Chu, W.S., Chen, X., Zou, C.W., and Wu, Z.Y. (2013). Growth and phase transition characteristics of pure M-phase VO_2 epitaxial film prepared by oxide molecular beam epitaxy. Appl. Phys. Lett. *103*, 131914.

29. Gupta, A., Narayan, J., and Dutta, T. (2010). Near bulk semiconductor to metal transition in epitaxial VO_2 thin films. Appl. Phys. Lett. *97*, 151912.

30. Vernardou, D., Pemble, M.E., and Sheel, D.W. (2004). Vanadium oxides prepared by liquid injection MOCVD using vanadyl acetylacetonate. Surf. Coatings Technol. *188–189*, 250–254.

31. Nistor, L.E., Rodmacq, B., Auffret, S., Schuhl, A., Chshiev, M., and Dieny, B. (2010). Oscillatory interlayer exchange coupling in MgO tunnel junctions with perpendicular magnetic anisotropy. Phys. Rev. B *81*, 220407.

32. Eyert, V. (2002). The metal-insulator transitions of VO_2: A band theoretical approach. Ann. Phys. *11*, 650–704.

33. Oleinik, I.I., Tsymbal, E.Y., and Pettifor, D.G. (2002). Atomic and electronic structure of Co/$SrTiO_3$/Co magnetic tunnel junctions. Phys. Rev. B *65*, 1–4.

34. Oleinik, I., Tsymbal, E.Y., and Pettifor, D. (2000). Structural and electronic properties of magnetic tunnel junction from first principles. Phys. Rev. B *62*, 3952–3959.

35. Goodenough, J.B. (1971). The two components of the crystallographic transition in VO_2. J. Solid State Chem. *3*, 490–500.

36. Yuasa, S., Fukushima, A., Kubota, H., Suzuki, Y., and Ando, K. (2006). Giant tunneling magnetoresistance up to 410% at room temperature in fully epitaxial Co/MgO/Co magnetic tunnel junctions with bcc Co(001) electrodes. Appl. Phys. Lett. *89*, 1–4.

37. Yin, H., Luo, M., Yu, K., Gao, Y., Huang, R., Zhang, Z., Zeng, M., Cao, C., and Zhu, Z. (2011). Fabrication and Temperature-Dependent Field-Emission Properties of Bundlelike

VO_2 Nanostructures. ACS Appl. Mater. Interfaces *3*, 2057–2062.

38. Kang, M., Kim, S.W., and Ryu, J.-W. (2015). Analysis of diverging effective mass extracted from thermoelectric power across the metal–insulator transition in VO_2. J. Appl. Phys. *118*, 035105.

39. Zhuravlev, M.Y., Tsymbal, E.Y., and Vedyayev, A. V. (2005). Impurity-Assisted Interlayer Exchange Coupling across a Tunnel Barrier. Phys. Rev. Lett. *94*, 026806.

40. Parkin, S.S.P., and Mauri, D. (1991). Spin engineering: Direct determination of the Ruderman-Kittel-Kasuya-Yosida far-field range function in ruthenium. Phys. Rev. B *44*, 7131–7134.

41. Kawatani, K., Takami, H., Kanki, T., and Tanaka, H. (2012). Metal-insulator transition with multiple micro-scaled avalanches in VO_2 thin film on TiO_2 (001) substrates. Appl. Phys. Lett. *100*, 173112.

42. Wang, X., Yang, Q., Wang, L., Zhou, Z., Min, T., Liu, M., and Sun, N.X. (2018). E-field Control of the RKKY Interaction in FeCoB/Ru/FeCoB/PMN-PT (011) Multiferroic Heterostructures. Adv. Mater. *30*, 1803612.

43. Morrison, V.R., Chatelain, R.P., Tiwari, K.L., Hendaoui, A., Bruhács, A., Chaker, M., and Siwick, B.J. (2014). A photoinduced metal-like phase of monoclinic VO_2 revealed by ultrafast electron diffraction. Science *346*, 445–448.

Figures and Tables

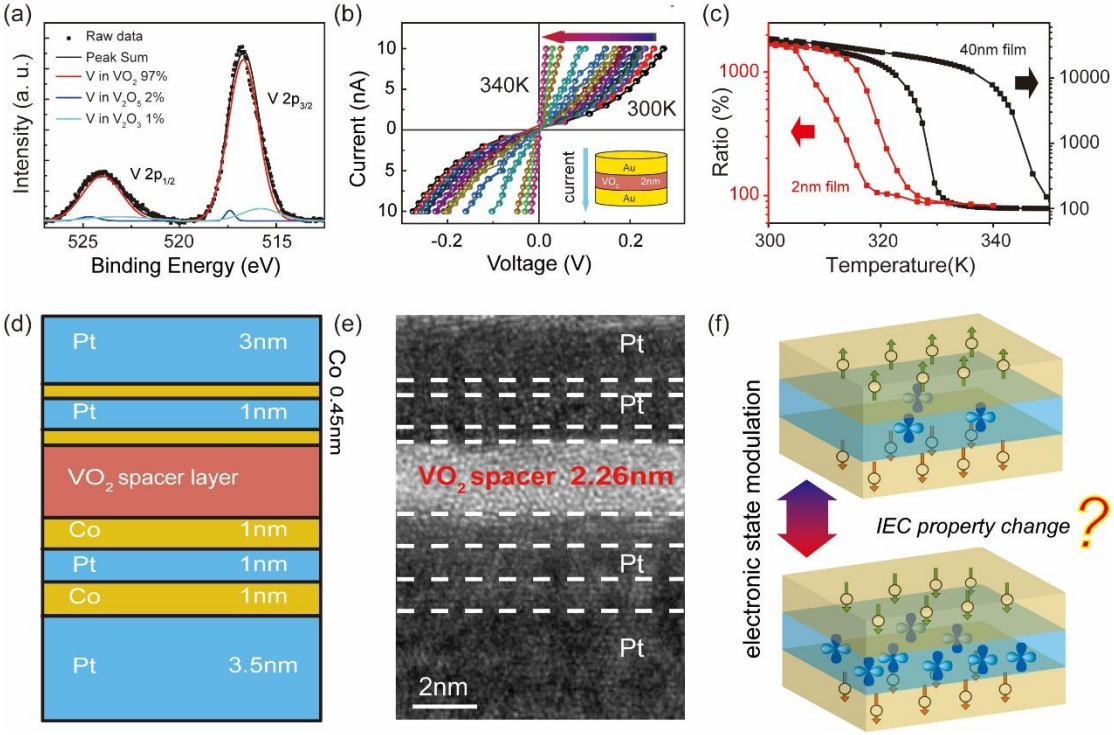

Figure 1. Atomically-thin VO_2 and magnetic heterostructures.

(A) X-ray photoelectron spectroscopy (XPS) profile of the sample with peak fitting results. The proportion of VO_2 reaches 97%.

(B) I-V curve of the VO_2 tunnel junction measured at different temperatures with the current flowing vertically through the device. The insert gives the schematic of the device which is fabricated based on Au/VO_2 (2 nm)/Au heterostructures with a diameter of 10 μm.

(C) The resistance change ratios versus temperature of 2-nm- and 40-nm-thick VO_2 films with a current of 10 nA, which indicate the existence of metal-insulator transition. The resistance change ratio is defined as the temperature dependent resistance divided by its minimum value.

(D) The schematic of the $[Pt/Co]_2/VO_2/[Co/Pt]_2$ heterostructures.

(E) High-resolution transmission electron microscopy (HRTEM) image of the $[Pt/Co]_2/VO_2$ (2.26 nm)/$[Co/Pt]_2$ sample with distinct interfaces.

(F) Schematic diagram of the spinterface-tailored interlayer exchange coupling (IEC) effect. The insulator to metal transition of VO_2 spinterface can enhance the electron density of 3d orbitals near Fermi surface, which may induce the evolution of the interlayer exchange coupling (IEC).

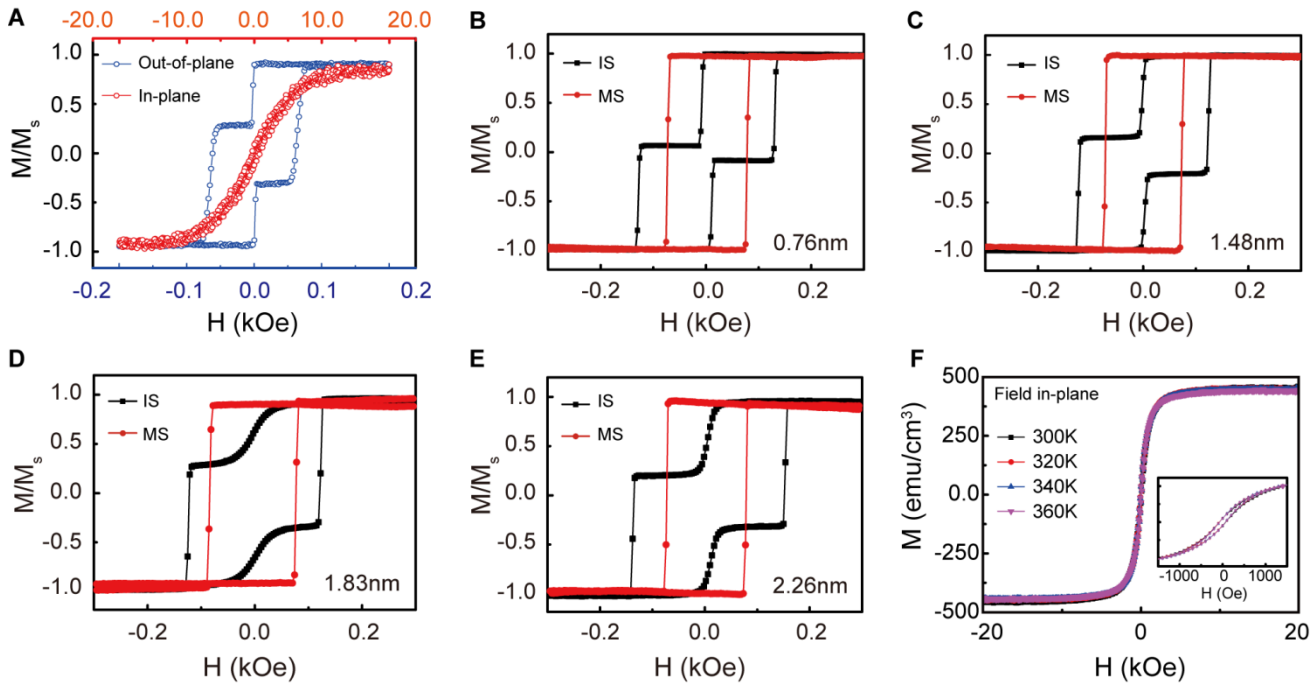

Figure 2. Magnetic properties of $[Pt/Co]_2/VO_2/[Co/Pt]_2$ heterostructures.

(A) Hysteresis loops of the $[Pt/Co]_2/VO_2$ (0.76 nm)/$[Co/Pt]_2$ sample measured by vibrating sample magnetometer (VSM) at room temperature with magnetic field applied in-plane (red line, step size 200Oe) and out-of-plane (blue line, step size 2 Oe), where *M* is the magnetization of the magnetic layers; M_S is the saturation magnetization, *H* is the external magnetic field.

(B)-(E) Hysteresis loops of the heterostructure samples measured by polar magneto-optic Kerr microscope (p-MOKE, measurement frequency 0.1 Hz) with VO_2 at insulating state (IS, 300 K, black line) and metallic state (MS, 360 K, red line), where the thickness of VO_2 spacer is 0.76, 1.48, 1.83 and 2.26 nm, respectively. The two magnetization flips merge into one after the insulator to metal transition.

(F) In-plane hysteresis loops of the $[Pt/Co]_2/VO_2$ (0.76 nm)/$[Co/Pt]_2$ sample at different temperatures measured by VSM (step size 100 Oe), which show no indication of anisotropy change in the metal-insulator transition. The inset gives the enlarged image from -1000 to 1000 Oe.

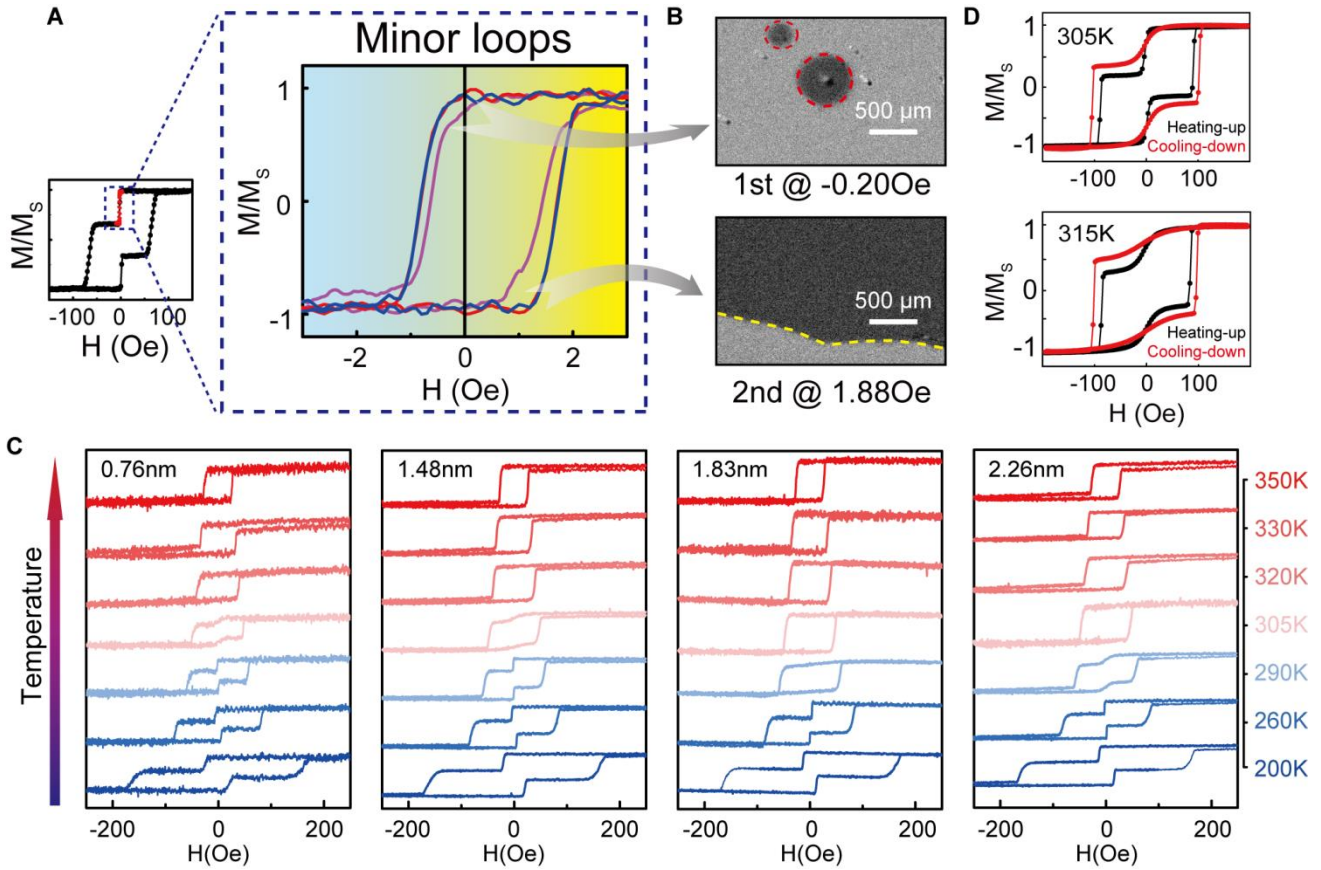

Figure 3. Regulation of IEC during metal-insulator transition process.

(A) Minor loops of $[Pt/Co]_2/VO_2$ (0.76 nm)/$[Co/Pt]_2$ sample obtained by VSM in the magnetic field range of ±3 Oe with a step of 0.1 Oe.

(B) Magnetic domain switching behavior of the sample around the minor loop field range obtained from Kerr microscope with out-of-plane field applied. The center deviation of minor loop indicates the existence of an AFM coupling.

(C) The variation of hysteresis loops measured by VSM (step size 0.5 Oe) at different temperatures for $[Pt/Co]_2/VO_2/[Co/Pt]_2$ samples with VO_2 of 0.76, 1.48, 1.83, 2.26 nm respectively. The loop features a smooth flip of the top FM layer before a sudden transition into one single flip, and the critical temperatures of IEC type change show obvious difference.

(D) The comparison of the hysteresis loops during heating-up and cooling-down process at 305 K and 315 K. The sharpness of the flip in both results shows a clear difference which is consistent with VO_2 hysteresis feature.

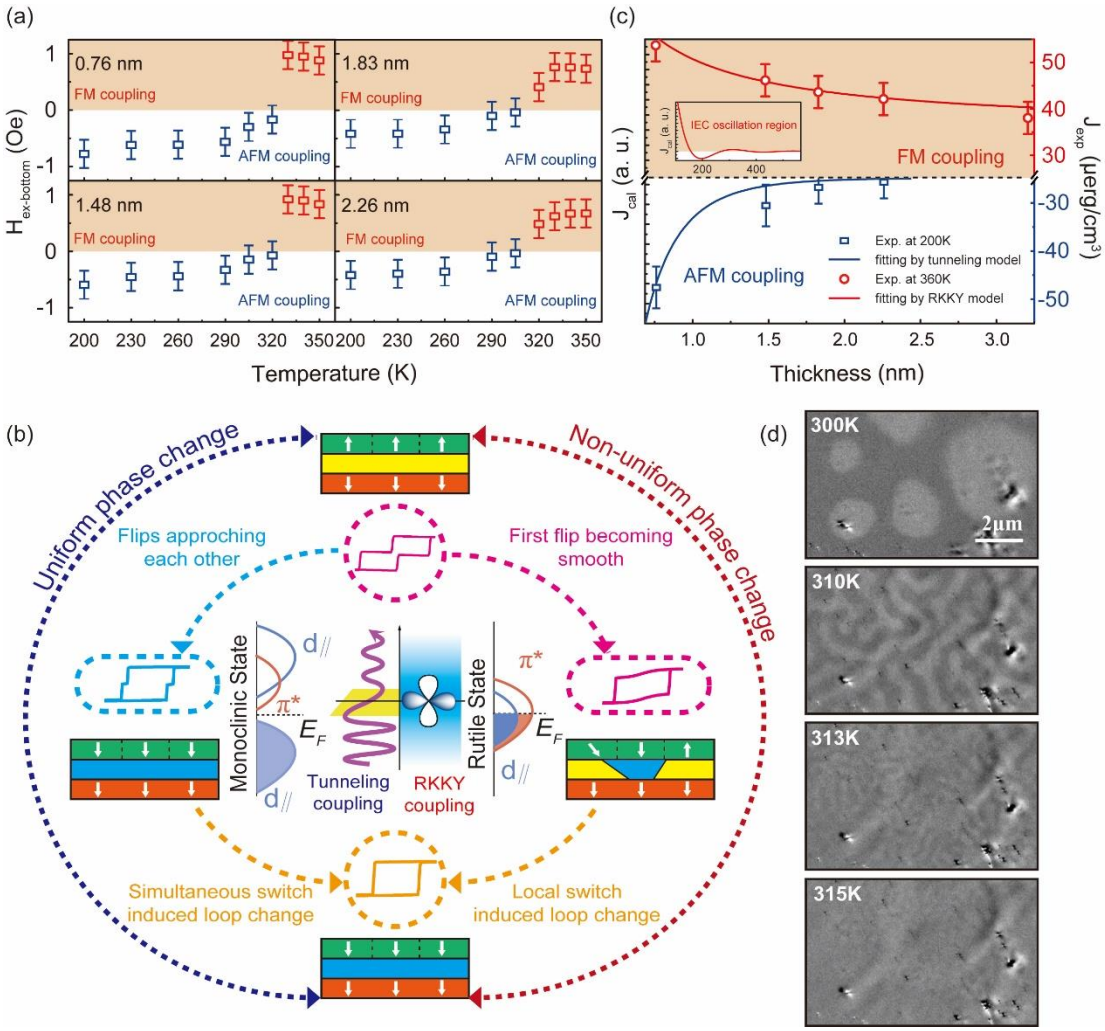

Figure 4. Mechanism of spinterface-tailored IEC via metal-insulator transition.

(A) Exchange bias field of bottom magnetic layer ($H_{ex\text{-}bottom}$) versus temperature for 0.76, 1.48, 1.83 and 2.26 nm VO_2, respectively.

(B) Thickness dependence of coupling strength obtained from experiment (J_{exp}) and calculation (J_{cal}) with insulating (at 200 K) and metallic (at 360 K) VO_2 spinterface, respectively. The solid blue line is a fitting curve according to the spin dependent tunneling theory with parameters of barrier height 1 eV, effective mass of m_{eff}=1m_e. The solid red line is a fitting curve following the RKKY theory with k_F=1.4*10^7 m^{-1}. Right Y axis has been broken from -25 to 25 μerg/cm^3. The inset gives the IEC oscillation calculated from the RKKY model over broad range of VO_2 thickness, which indicates the characteristics of an extremely large oscillation period (up to hundreds of nanometers).

(C) Schematic diagram of the IEC regulation mechanism. The inner image gives the energy band variation of VO_2 and corresponding coupling mechanism before and after the insulator to metal transition. The spectral weight transfer from π* (d_{xy}) orbitals into the valence $d_{//}$ ($d_{xz,\ yz}$) orbitals enhances the electron density near Fermi surface, and makes coupling mechanism change from the spin dependent tunneling to RKKY interaction. The outside gives the different

spin dynamic evolution process with uniform (left arrow) and non-uniform (right arrow) phase change. For the non-uniform phase change, the electric domain in VO_2 may induce local magnetic domain switching during the metal-insulator transition.
(D) The magnetic domain morphology of 0.76-nm-thick VO_2 film observed by Kerr microscope at different temperatures with an applied field of 2.6 Oe.